*Applied Chemical Engineerings (2022) Volume 5 Issue 2*
doi:10.24294/ace.v5i2.1642

## Original Research Article

# Aluminum doping and lithium tungstate surface coating double effect to improve the cycle stability of lithium-rich manganese-based cathode materials

**Xuqiang Ren, Donglin Li*, Zhenzhen Zhao, Guangqi Chen, Kun Zhao, Xiangze Kong, Tongxin Li**

*School of Materials Science and Engineering, Chang'an University, Xi'an 710061, Shaanxi Province, China. E-mail: dlli@chd.edu.cn*

## ABSTRACT

Al doped lithium-rich manganese-based $Li_{1.2}Mn_{0.54-x}Al_xNi_{0.13}Co_{0.13}O_2$ ($x$ = 0, 0.03) cathode materials for lithium-ion batteries were synthesized with sol-gel method, and then $Li_2WO_4$ coating was prepared by one-step liquid phase method. The effects of Al doping and $Li_2WO_4$ coating on the electrochemical properties of lithium-rich manganese-based cathode materials were systematically studied. The results show that Al doping significantly improves the cycle stability of lithium-rich manganese-based cathode material, and the coating $Li_2WO_4$ significantly improves its magnification performance and the voltage attenuation of discharge plateau. The coating amount of $Li_2WO_4$ is 5%, and the specific capacity of $Li_{1.2}Mn_{0.51}Al_{0.03}Ni_{0.13}Co_{0.13}O_2$ cathode material is still up to about 110 mAh·g$^{-1}$ in the charge and discharge voltage range of 2.0–4.8 V and the current density of 1,000 mA·g$^{-1}$. At the same time, the capacity retention rate of 300 cycles at the current density of 100 mA·g$^{-1}$ is 78%, and the voltage attenuation of the discharge plateau during the cycle is also significantly reduced. This work provides a new idea for solving the cycle stability and platform voltage attenuation of lithium-ion battery lithium-rich manganese-based cathode materials.

***Keywords:*** Lithium-Ion Battery; Sol-Gel Method; Lithium-Rich Manganese-Based Cathode Material; $Li_2WO_4$; Al Doping

**ARTICLE INFO**

Received: 8 June 2022
Accepted: 22 August 2022
Available online: 7 September 2022



## 1. Introduction

High energy density lithium-ion batteries have always been the goal pursued by people in aspects of the mobile terminals, electric vehicles and others. In the existing battery technology, commercial graphite cathode materials have a discharge capacity of more than 350 mAh·g$^{-1}$, while the cathode material is only 140–170 mAh·g$^{-1}$. Therefore, the main factor limiting the energy density of lithium-ion batteries is the cathode material[1]. At present, the commercial cathode materials mainly include: $LiFePO_4$, $LiCoO_2$, etc. $LiFePO_4$ has good safety performance and stable circulation, but its theoretical capacity of 170 mAh·g$^{-1}$ barely satisfy the endurance requirements for long-range electric vehicles. It has disadvantages such as high price, shortage of cobalt resources, environmental pollution and so on[2–5]. To solve these problems and better meet the mileage requirements of electric vehicles, the layered lithium-rich manganese-based cathode material $xLi^2MnO^3(1-x)LiMO_2$ ($0 < x < 1$, M = Mn, Co, Ni...) can be considered as a solid solution or composite oxide composed of $LiMO_2$ (M = Mn, Co, Ni) and $Li_2MnO_3$. It is expected to become the cathode material of the next generation of lithium-ion batteries because of its high discharge specific

capacity greater than 250 mAh·g$^{-1}$ and high discharge plateau[6]. However, the lithium-rich manganese-based cathode material has poor cycle stability, low coulomb efficiency for the first charge and discharge, and poor rate performance. The most important thing is that the problem of rapid voltage attenuation of its discharge plateau has not been effectively solved, which limits its application[7].

The poor performance of lithium-rich manganese-based cathode materials is due to the surface phase transition and structural instability during charge and discharge[8]. At present, the research on them mainly focuses on element doping modification and surface coating. Doping modification of elements can improve the structural stability of cathode materials, reduce the obstruction of $Li^+$ migration and inhibit adverse phase transition, so as to improve the electrochemical performance of materials[9,10]. Common doped ions are mainly cations, such as $Na^{+}$[11], $K^{+}$[12], $Mg^{2+}$[13], $Ru^{4+}$[14], $Ti^{4+}$[15] and $Mo^{6+}$[16,17]. At the same time, there are also anionic doping such as $F^{-}$[18] and $S^{2-}$[19]. $Mg^{2+}$ and $F^{-}$ can also be used for doping of anions and anions[20]. It is worth mentioning that surface coating can prevent lithium-rich manganese-based materials from directly contacting with electrolyte to damage the structure of materials, therefore reduce the occurrence of side reactions, and then improve the electrochemical performance of materials[21]. Common surface coatings include $ZrO_2$[22], $TiO_2$[23], $Al_2O_3$[24] and other oxides, as well as $AlF_3$[25], $AlPO_4$[26], $LaF_2$[27] and C[28] etc., but it's difficult to use these coating materials to greatly improve the platform attenuation. Therefore, it is necessary to further study and find other coating materials. Doping and coating modified materials are related to the synthesis method. Lithium-rich manganese-based cathode materials can be synthesized with methods of high-temperature solid-state[29], coprecipitation[30], sol-gel[31], hydrothermal[32]. The synthesis conditions also have an important impact on the structure and electrochemical properties of lithium-rich manganese-based materials. Sol-gel can achieve atomic level uniform mixing. Moreover, it has the advantages of simple operation, low sintering temperature, small and uniform particle size of products, large specific surface area and so on. In view of this, Song *et al.*[31] synthesized $Li_{1.2}Mn_{0.54}Ni_{0.13}Co_{0.13}O_2$ by sol-gel method. After 100 cycles at 400 mA·g$^{-1}$ current density, it still has a specific capacity of 133.7 mAh·g$^{-1}$, and the capacity retention rate is 84.14%.

Li *et al.*[33,34] doped Al into lithium-rich manganese-based cathode material by sol-gel method, which effectively improved its cycle performance. The research shows that Al doping can stabilize the crystal structure of lithium-rich manganese-based cathode material, improve the cycle performance, promote charge transfer and reduce impedance, and improve the rate performance of lithium-rich manganese-based cathode material. At the same time, existing studies have shown that $Li_2WO_4$ has good $Li^+$ conductivity[35,36]. Hayashi *et al.*[37–39] deposited amorphous $Li_2WO_4$ on the surface of $LiCoO_2$ cathode material, which can reduce the interface resistance of lithium-ion batteries, and can prevent the electrolyte from directly contacting the cathode material, reduce side reactions, and then improve its electrochemical performance. However, there are few reports on $Li_{1.2}Mn_{0.54}Ni_{0.13}Co_{0.13}O_2$ surface modification of $Li_2WO_4$ at present. Therefore, the $Li_{1.2}Mn_{0.54}Ni_{0.13}Co_{0.13}O_2$ cathode material was simultaneously modified by Al doping and $Li_2WO_4$ surface coating in this work. The results show that the $Li_{1.2}Mn_{0.54}Ni_{0.13}Co_{0.13}O_2$ coated with 5% $Li_2WO_4$ has good rate performance; the capacity retention rate can reach 78% after 300 cycles at a current density of 100 mA·g$^{-1}$, and the specific capacity is still 150 mAh·g$^{-1}$. The capacity retention rate of pure Li-rich manganese-based cathode materials is only 60.4%. More importantly, the coating layer also significantly improves the rate performance and the attenuation of the discharge plateau. This provides an idea for future research on Li-rich manganese-based cathode materials.

## 2. Results and discussion

### 2.1 X-ray diffraction analysis

**Figure 1** shows the XRD diffraction patterns of three materials (for convenience, $Li_{1.2}Mn_{0.54}Ni_{0.13}Co_{0.13}O_2$, $Li_{1.2}Mn_{0.51}Al_{0.03}Ni_{0.13}Co_{0.13}O_2$ and 5% $Li_2WO_4$@$Li_{1.2}Mn_{0.51}Al_{0.03}Ni_{0.13}Co_{0.13}O_2$ are rec-

orded as LMNC-1, LMNC-2 and LMNC-3 respectively) and the standard card PDF#22-0693 of $Li_2WO_4$ with $R\bar{3}m$ spatial structure group. It can be seen from the figure that the three materials have all the characteristic peaks of lithium-rich manganese-based materials, belonging to the trilateral system, $R\bar{3}m$ space group[17,18]. At the position of $2\theta$ = 20°–25°, there are some diffraction peaks with weak intensity, which are caused by the ordering of Li and Mn superlattices. The composition of $Li_2MnO_3$ is determined (space group: $C2/m$) exists, which is consistent with the previous research of Xiang *et al.*[11–15] It can be seen that the diffraction peaks of (006)/(102) and (018)/(110) crystal planes have obvious splitting, which is due to the oxygen sublattice of the $\alpha$-$NaFeO_2$ layered structure in $LiMO_2$, which shows that the material modified by doping and coating still has a good $\alpha$-$NaFeO_2$ layered structure without changing the original Li-rich manganese-based material with some electrochemically active phase structures[40–43]. Comparing the standard cards of $Li_2WO_4$, it is found that LMNC-3 has very obvious diffraction peaks on (111), (210), (211), (220), (300), (310), (410), (331), (420), (521) and (440) crystal planes, which proves that $Li_2WO_4$ is successfully wrapped on lithium-rich materials. Since the radii of $Al^{3+}$ and $Mn^{4+}$ are the same (both 0.053 nm), the XRD structures of LMNC-1 and LMNC-2 were refined to prove that Al is doped in the manganese position (**Figure 2**). In the figure, $R_{wp}$ is the reliability factor and $CHI^2$ is the goodness of fit. The refined results show that the $R_{wp}$ = 3.92%, $CHI^2$ = 1.343 of LMNC-1, and the $R_{wp}$ = 4.41%, $CHI^2$ = 1.706 of LMNC-2. This is in line with the reliable judgment standard of refined results: $R_{wp}$ < 10%, $CHI^2$ < 2[44]. It can be concluded that Al is indeed doped at the manganese site.

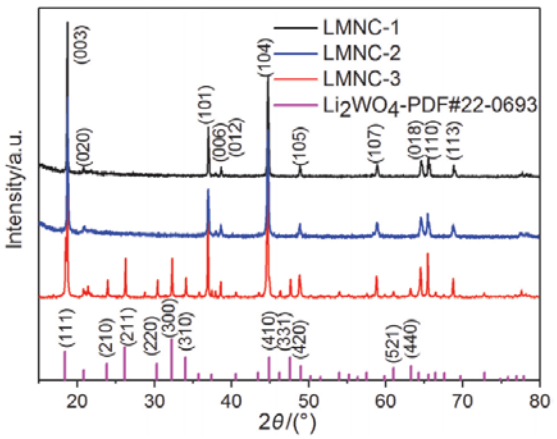


**Figure 1.** X-ray diffraction patterns for the LMNC-1, LMNC-2 and LMNC-3 samples.

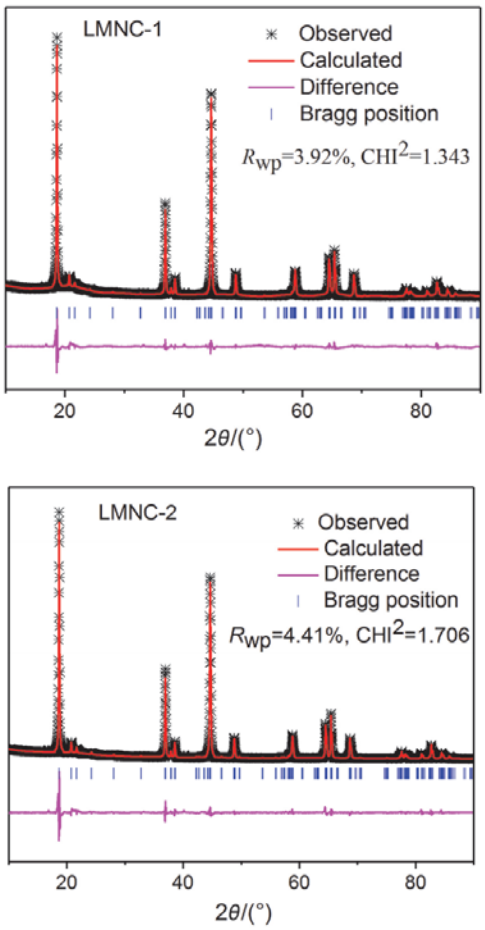


**Figure 2.** Rietveld refinement results for XRD data.

## 2.2 Analysis of electrode material morphology

**Figure 3** is the scanning electron microscope (SEM) of the three materials. It can be seen from **Figures 3b**, **3d** and **3f** that the uncoated LMNC particles are uniform and have obvious agglomeration. The small particles of the three materials agglomerate together to form secondary particles, which is conducive to the wetting of electrolyte and makes $Li^+$ easier to diffuse into the materials. From the **Figures 3a**, **3c** and **3e**, it is found that LMNC-1 and LMNC-2 materials without $Li_2WO_4$ coating have sharp edges and corners, and the particle size is 150–300 nm. However, after coating $Li_2WO_4$, the size of the material has increased to about 500 nm, and the surface edges and corners of the material are not obvious, and it is relatively smooth. It can also be seen that small particles of about 10 nm are attached, which is due to that the liquid phase coating method cannot uniformly coated $Li_2WO_4$ on the surface of all lithium-rich manganese-based cathode

particles to form $Li_2WO_4$ particles, which also indicates that $Li_2WO_4$ is on the surface of lithium-rich manganese-based cathode materials.

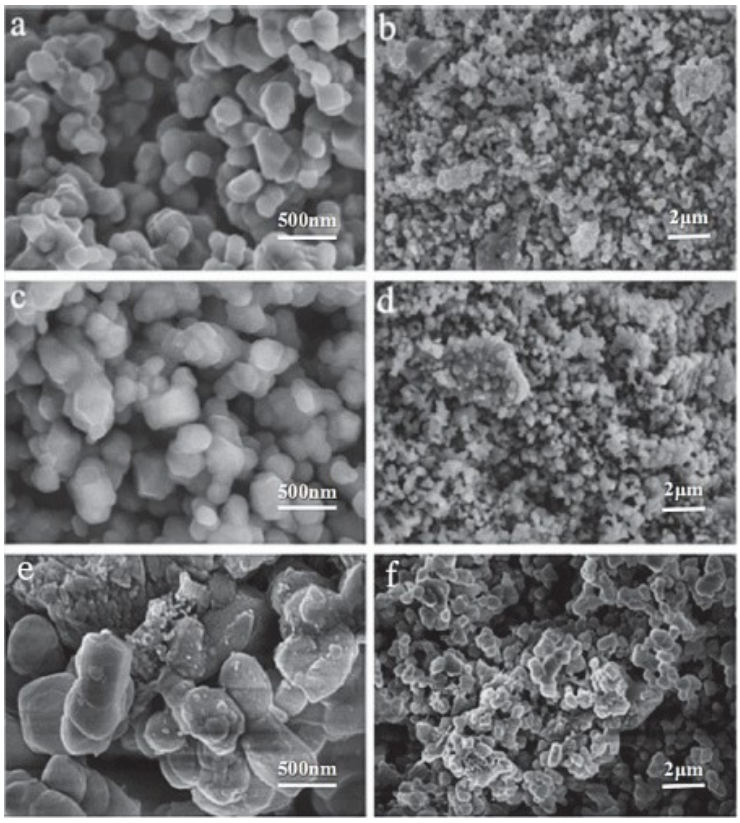


**Figure 3.** SEM photographs of LMNC-1 (**a**, **b**), LMNC-2 (**c**, **d**) and LMNC-3 (**e**, **f**) materials.

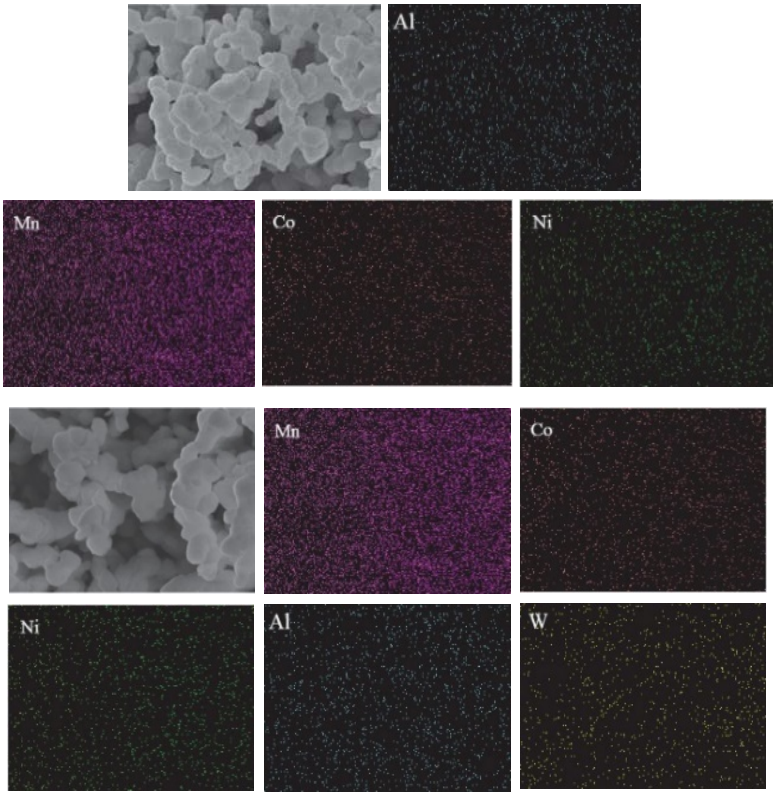


**Figure 4.** EDS photo of LMNC-2 and LMNC-3 materials.

**Figures 4a** and **4b** are the EDS analysis results of LMNC-2 and LMNC-3 materials respectively. By selecting a part in the sample for scanning analysis, it can be found that Mn, Ni, Co, Al are evenly distributed in the material particles, and there is no element segregation. In **Figure 4b**, W element is also evenly distributed in the material particles. Combined with SEM, EDS and XRD, it can be shown that Al element is uniformly doped in LMNC material, and $Li_2WO_4$ is well coated on the surface of the doped material.

## 2.3 Electrochemical performance analysis

In **Figures 5a**, 5**b**, and 5**c** are the charge discharge curves of the three materials under different current densities. During the first cycle of charge and discharge, the voltage from the initial voltage to about 4.4 V is the separation of $Li^+$ in $LiMO_2$, while the transition metal ion $Ni^{2+}$ is oxidized to $Ni^{4+}$ and $Co^{3+}$ is oxidized to $Co^{4+}$. In this process, $Li^+$ in $LiMnO_3$ also diffuses to $LiMO_2$, which has lost $Li^+$; when the voltage is charged to about 4.5 V, irreversible structural changes occur in the lattice of the material. At this time, $LiMnO_3$ losing Li is activated into $MnO_2$, and $MnO_2$ will also provide corresponding capacity during the discharge process. This is also the typical first cycle charge discharge curve of lithium-rich manganese base[41]. The similar curves of the three materials can explain that the doped and coated materials have not changed the phase structure of the original lithium-rich manganese base materials. It can be seen from the figure that the first discharge specific capacity of LMNC-1, LMNC-2 and LMNC-3 materials are 274.7, 253.0 and 260.7 $mAh \cdot g^{-1}$ respectively, and the corresponding first charge and discharge efficiency is 72%, 70% and 73%. The first charge and discharge efficiency of Al doped materials is not improved, because Al itself is non electrochemical active. However, the first charge and discharge efficiency of the coated material is slightly improved because $Li_2WO_4$ has good $Li^+$ conductivity, ensuring more $Li^+$ disembedding. Combined with the cycle diagram **Figure 5d** of different magnification, it can be seen that the specific discharge capacity will be reduced after Al doping, because Al doping replaces Mn and reduces the substances with redox activity[45], and as the radius of $Al^{3+}$ is similar to that of $Co^{3+}$, a small amount of Al will replace the position of Co, which will also reduce the specific discharge capacity of the material. However, at 1C and 2C magnification, Al doping has significantly higher specific capacity, which is due to the reduced cell parameters of Al doping, stabilizing the structure of the material, and ensuring the insertion of more lithium-ions[42].

It can be seen from **Figure 5d** that the material with double effect modification of Al doping and $Li_2WO_4$ coating at the same time has a higher specific capacity, and a discharge specific capacity of nearly 70 $mAh \cdot g^{-1}$ at 10C. This is because $Li_2WO_4$ can reduce the interface impedance, and it also has good conductivity of $Li^+$, which can accelerate $Li^+$ disembedding, ensure that more $Li^+$ participate in the electrochemical reaction, and improve the magnification performance of the material. This also corresponds to the LMNC-3 mentioned later, which has the minimum interface impedance[37–39] (**Figure 8**). It is important that lithium-rich manganese base should pay more attention to the attenuation of discharge plateau. **Figures 5e** and **5f** are the platform comparison diagrams of LMNC-1, LMNC-2 and LMNC-3 at 0.2C and 2C respectively. From **Figure 5e**, it can be found that the charging platform of LMNC-3 is the lowest and the discharging platform is the highest, which is conducive to the disembedding of $Li^+$ in the material. It is found from the **Figure 5f** that the large magnification is more obvious at 2C. The unmodified material has almost no discharge plateau and the specific capacity is also very low, while LMNC-3 has an obvious discharge plateau, and the specific capacity is still 150 $mAh \cdot g^{-1}$. This is because the material structure is stabilized after Al doping and $Li_2WO_4$ coating double effect modification, which is further explained by the differential capacitance curve in the following text (**Figure 7**).

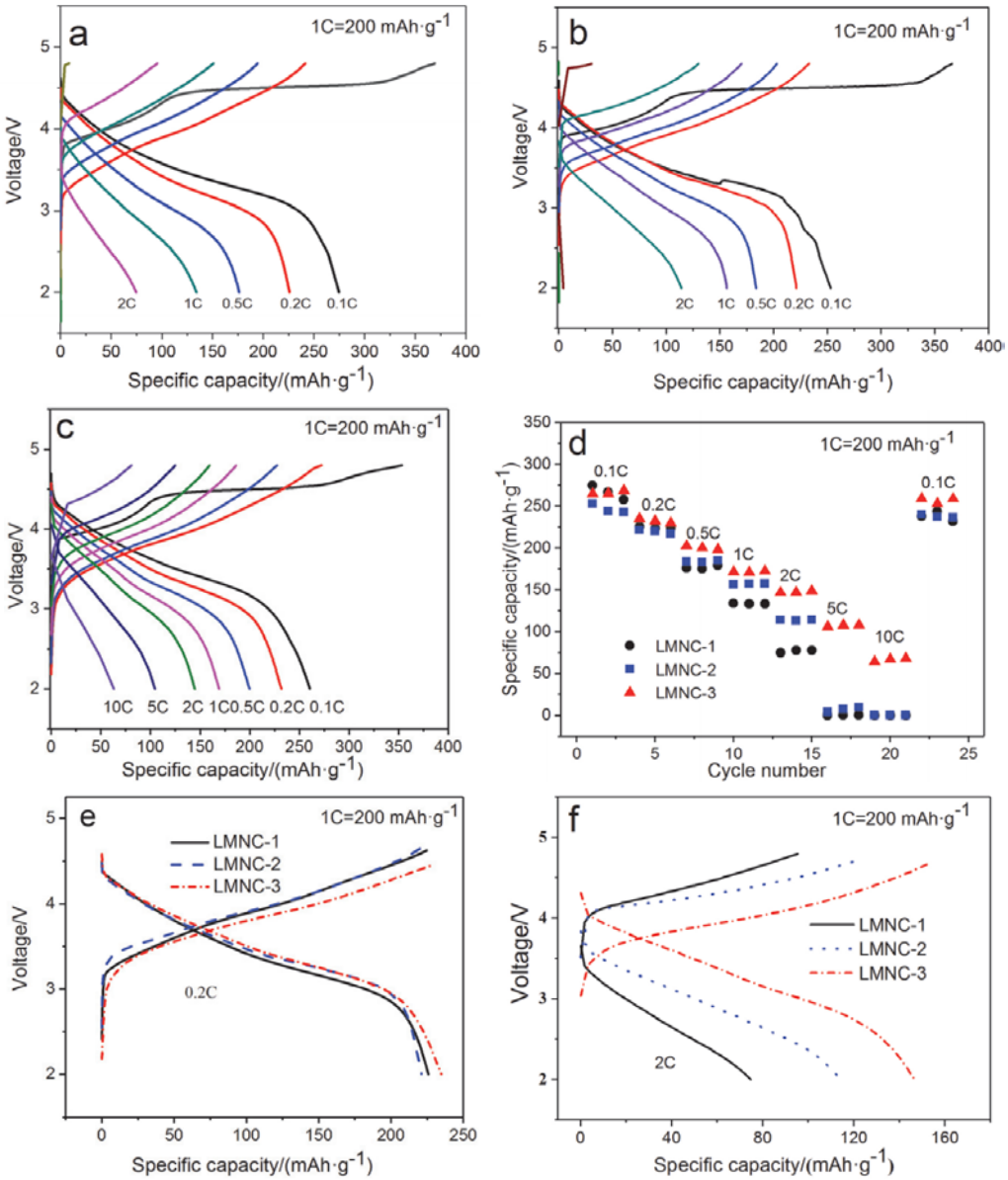


**Figure 5.** Charge and discharge curves of LMNC-1 (**a**) LMNC-2 (**b**) and LMNC-3 (**c**) at different magnifications; (**d**) comparison of the performance of the three materials at rates; (**e**) and (**f**) platform comparison of the three materials at 0.2C and 2C.

**Figure 6a** is a comparison diagram of the long cycle performance of LMNC-1, LMNC-2 and LMNC-3 materials at 0.5C and the platform attenuation under different cycle times. It can be seen from the **Figure 6a** that after 300 cycles, the capacity of the three materials is decreasing, and the capacity retention rates of the three materials are 60.0%, 82.0% and 78.0% respectively. The unmodified capacity retention rate is the lowest. At the same time, the capacity of doped and coated LMNC-3 is reduced from 195 mAh·g$^{-1}$ to 151mAh·g$^{-1}$, while the capacity retention rate of doped LMNC-2 is high, but the capacity is reduced from 167 mAh·g$^{-1}$ to 137 mAh·g$^{-1}$, which is lower than that of LMNC-3. In order to further illustrate the effect of double effect modification on the cycle, **Figure 5b** compares the platform attenuation of LMNC-1, LMNC-2 and LMNC-3 at 0.5C for 150 cycles. It can be found from the figure that the platform of LMNC-3 is slightly higher in the first cycle, and the modified LMNC-3 has a higher platform after 150 cycles, while the platform of LMNC-2 only doped with Al after 150 cycles is similar to that of LMNC-1. This shows that $Li_2WO_4$ coating slows down the attenuation of platform voltage of lithium-rich manganese-based materials. As we all know, the voltage attenuation of the discharge plateau of lithium-rich manganese-based

materials is mainly due to the transformation of the material surface from layered structure to spinel structure, resulting in the phase transition, resulting in the blockage of $Li^+$ transmission channel, and then the voltage attenuation. By doping and stabilizing the crystal structure of the material, the coating of the material surface inhibits the transformation of lithium-rich spinel and slows down the attenuation of the discharge voltage platform[15,25].

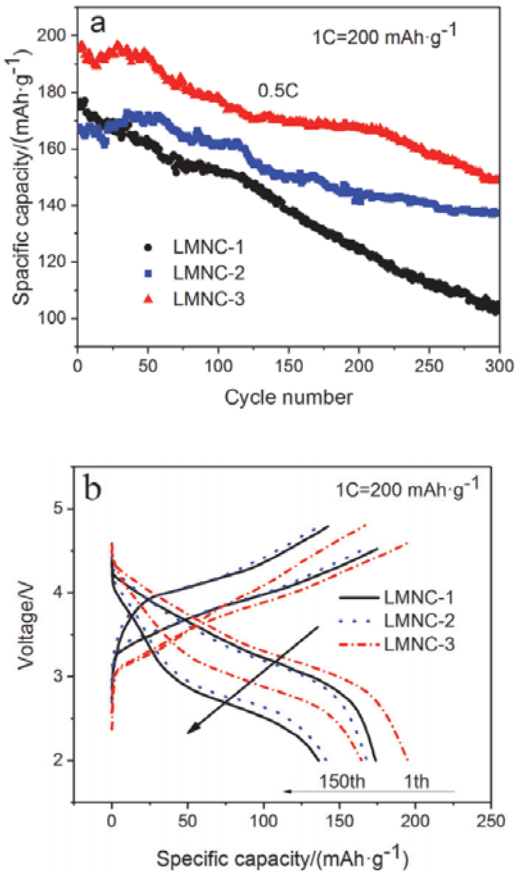


**Figure 6.** (**a**) cyclic comparison of three materials at a current density of 0.5C; (**b**) platform comparison.

As for the reasons why Al doping improves the cycle stability of lithium-rich manganese-based materials, studies have shown that Al replaces Mn in the position of Al doped lithium-rich manganese-based materials, stabilizing the structure of the materials, and inhibiting the transfer of spinel phase in the electrochemical reaction process of the materials due to the charge transfer effect, thereby improving the cycle performance of the materials[33,34,42]. Coating $Li_2WO_4$ can improve the attenuation of the platform, which is due to the improvement of $Li^+$ conductivity[35,36] after coating $Li_2WO_4$, which is more conducive to $Li^+$ disembedding. In order to further prove the function of its coating, **Figure 7** is a comparison diagram of the differential capacitance curve of LMNC-2 and LMNC-3 after the first cycle and 150 cycles under the current density of 0.5C. It can be found that the discharge plateau of LMNC-3 coated with $Li_2WO_4$ is significantly higher, and the attenuation is relatively slow. In addition, it can be found that the potential difference of LMNC-2 is about 0.56 V, while the potential difference of LMNC-3 is only about 0.34 V. Therefore, it can be explained that the polarization of the coated material is significantly reduced, which is conducive to improving the electrochemical performance of the material.

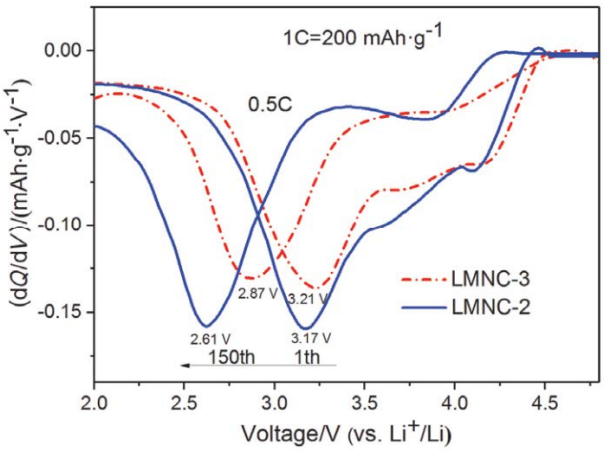


**Figure 7.** Comparison of dQ/dV curves between LMNC-2 and LMNC-3.

**Figure 8** shows the electrochemical impedance diagrams (EIS) of the three materials after 300 cycles. By observing the Nyquist diagram, it can be found that the three materials are all composed of semicircle parts in the high-frequency region and diagonal parts in the low-frequency region. The fitted equivalent circuit diagram is composed of the following parts: ohmic impedance $R_s$ of electrolyte and diaphragm, charge transfer impedance $R_{ct}$, constant phase angle element CPE, Warburg impedance $Z_w$. First, $R_{ct}$ is connected in parallel with CPE, then $Z_w$ is connected in series, and finally $R_s$ is connected in series. The semicircle diameters of the three materials in the high-frequency region from small to large are LMNC-3, LMNC-2 and LMNC-1 in turn, indicating that the modified materials improve the electronic conductivity of the materials. It can be

found from the low-frequency region that the slope of LMNC-3 is the largest, indicating that the diffusion rate of $Li^+$ in the modified material is greater. This is because Al doping not only stabilizes the material structure, but also reduces the interface impedance by surface reconstruction[46], and $Li_2WO_4$ has good $Li^+$ conductivity after coating[37–39].

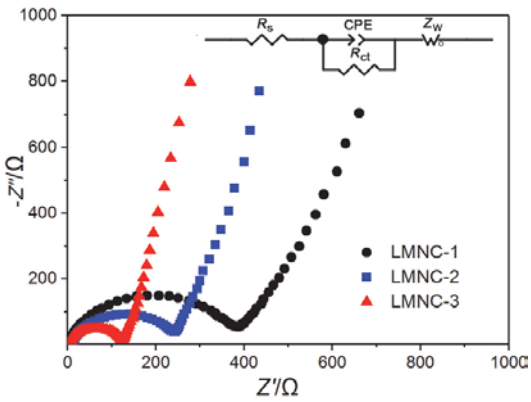


**Figure 8.** Nyquist curves of LMNC-1, LMNC-2 and LMNC-3 after 300 cycles.

# 3. Conclusion

After Al doping and $Li_2WO_4$ coating of lithium-rich manganese base were successfully carried out by sol-gel method, the rate performance of the material was improved, the long cycle stability was improved, and the problem of platform attenuation was alleviated. It is proved that Al doping can stabilize the crystal structure of the material, so as to improve the magnification and cycle performance of lithium-rich manganese-based materials. Coating $Li_2WO_4$ can obviously improve the magnification performance of the material and slow down the attenuation of the platform, because $Li_2WO_4$ has good $Li^+$ conductivity, and after coating, it also reduces the battery interface impedance and protects the material from electrolyte corrosion, reducing the internal polarization of the material. This work provides a new idea and direction for the research of lithium-rich manganese-based modification in the future.

# 4. Experiment part

## 4.1 Synthesis of materials

According to the stoichiometric ratio of lithium-rich manganese-based $Li_{1.2}Mn_{0.54-x}Al_xNi_{0.13}Co_{0.13}O_2$ cathode material, $CH_3COOLi{\cdot}2H_2O$, $(CH_3COO)_2Mn{\cdot}4H_2O$, Ni $(CH_3COO)_2{\cdot}4H_2O$, $CO(CH_3COO)_2{\cdot}4H_2O$, $Al(NO_3)_3{\cdot}9H_2O$ (in which $CH_3COOLi{\cdot}2H_2O$ is 5% excessive; take $x$ = 0 and 0.03) is stirred with water until it is completely dissolved, and then an appropriate amount of sucrose is added to stir and coordinate for 1–2 hours. Then evaporate the solvent in 85 ℃ water bath to form purple transparent sol, and finally place the sol in 100 ℃ oven for drying. The dry gel was ground into powder, and the heat treatment was carried out in two steps. First, it was calcined at 450 ℃ in air for 5 hours, and then calcined at 900 ℃ in air for 12 hours to obtain the corresponding lithium-rich cathode material.

Take the prepared $Li_{1.2}Mn_{0.51}Al_{0.05}Ni_{0.13}Co_{0.13}O_2$, add it to the prepared mixed solution of $(NH_4)_{10}W_{12}O_{41}{\cdot}xH_2O$ and $CH_3COOLi{\cdot}2H_2O$, and then disperse it with ultrasound for 30 minutes, then keep it under negative pressure for 5 to 10 hours, then evaporate the solvent, dry it, compact it, and calcine it in air at 650 ℃ for 6 hours to get 5% $Li_2WO_4@Li_{1.2}Mn_{0.51}Al_{0.03}Ni_{0.13}Co_{0.13}O_2$.

## 4.2 Material characterization

Bruker D8 Advance X-ray diffractometer (XRD) made in Germany was used to analyze the phase of the sample. Cu target Kα is taken as a radiation source, $\lambda$ = 0.15406 nm, the tube current is 40 mA, the tube voltage is 40 kV, and the scanning range is $10° \leq 2\theta \leq 90°$, the scanning speed is 10.0 (°)/min, and the step size is 0.02°. The morphology of the synthesized samples was analyzed by JSM-4800 field emission scanning electron microscope FESEM. The working voltage was 5kV and the working current was 0.01 mA.

## 4.3 Material electrochemical performance test

The prepared LMNC-1, LMNC-2 and LMNC-3 are used as positive active substances, super P-KS 6 (mass ratio of 1:1) is used as conductive agent, polyvinylidene fluoride (PVDF) is used as adhesive, and they were added to an appropriate amount of *N*-methyl pyrrolidone (NMP) dispersant according to the mass ratio of 7:2:1. Then it was

mixed and stirred evenly to make slurry, coated on the collector aluminum foil, and then the coated electrode is dried at 100 °C constant temperature for 12 hours in argon atmosphere. The dried electrode sheet was used as the positive electrode, the lithium metal sheet as the counter electrode, the polypropylene microporous membrane (Celgard 2400) as the diaphragm, and 1 mol·L$^{-1}$ $LiPF_6$ methyl ethyl carbonate (DMC)-ethylene carbonate (EC)-methyl ethyl carbonate ($V_{DMC}$:$V_{EC}$:$V_{EMC}$ = 1:1:1) as the electrolyte. The charge discharge performance and long cycle performance at different magnification were tested by Xinwei charge discharge tester at room temperature, in which the charge discharge voltage range was 2.0–4.8 V, and the current density 1C = 200 mA·g$^{-1}$. The electrochemical impedance spectroscopy (EIS) of materials was tested by Princeton electrochemical workstation.

## Acknowledgements

This project is supported by the National Natural Science Foundation of China (Nos. 21473014, 21073021).

## Conflict of interest

The authors declare no conflict of interest.

## References

1. Tarascon JM, Armand M. Issues and challenges facing rechargeable lithium batteries. Nature 2001; 414: 359–367.
2. Armand M, Tarascon JM. Building better batteries. Nature 2008; 451: 652–657.
3. Park KS, Cho MH, Jin SJ, *et al*. Effect of Li ion in transition metal sites on electrochemical behavior of layered lithium manganese oxides solid solutions. Solid State Ionics 2004; 171(1–2): 141–146.
4. Kang K, Meng YS, Breger J, *et al*. Electrodes with high power and high capacity for rechargeable lithium batteries. Science 2006; 311: 977–980.
5. Fergus JW. Ceramic and polymeric solid electrolytes for lithium-ion batteries. Journal of Power Sources 2010; 195(15): 4554–4569.
6. Mohanty D, Kalnaus S, Meisner RA, *et al*. Structural transformation in a $Li_{1.2}Co_{0.1}Mn_{0.55}Ni_{0.15}O_2$ lithium-ion battery cathode during high-voltage hold. RSC Advances 2013; 3: 7479–7485.
7. Gallagher KG, Croy JR, Balasubramanian M, *et al*. Correlating hysteresis and voltage fade in lithium- and manganese-rich layered transition-metal oxide electrodes. Electrochemistry Communications 2013; 33: 96–98.
8. Croy JR, Gallagher GK, Balasubramanian M, *et al*. Examining hysteresis in composite $xLi_2MnO_3{\cdot}(1-x)LiMO_2$ cathode structures. The Journal of Physical Chemistry C 2013; 117: 6525.
9. Liu S, Liu Z, Shen X, *et al*. Li–Ti cation mixing enhanced structural and performance stability of Li-rich layered oxide. Advanced Engineering Materials 2019; 9(32): 1901530.
10. Zhang JN, Li Q, Ouyang C, *et al*. Trace doping of multiple elements enables stable battery cycling of $LiCoO_2$ at 4.6 V. Natural Energy 2019; 4: 594–603.
11. He W, Yuan DD, Qian JF, *et al*. Enhanced high-rate capability and cycling stability of Na-stabilized layered $Li_{1.2}[Co_{0.13}Ni_{0.13}Mn_{0.54}]O_2$ cathode material. Journal of Materials Chemistry A 2013; 1: 11397.
12. Li Q, Li G, Fu C, *et al*. $K^+$-doped $Li_{1.2}Mn_{0.54}Co_{0.13}Ni_{0.13}O_2$: A novel cathode material with an enhanced cycling stability for lithium-ion batteries. ACS Applied Materials & Interfaces 2014; 6(13): 10330–10341.
13. Xiang Y, Li J, Wu X, *et al*. Synthesis and electrochemical characterization of Mg-doped Li-rich Mn-based cathode material. Ceramics International 2016; 42: 8833.
14. Knight JC, Nandakumar P, Kan WH, *et al*. Effect of Ru substitution on the first charge–discharge cycle of lithium-rich layered oxides. Journal of Materials Chemistry A 2015; 3: 2006–2011.
15. Deng ZQ, Manthiram A. Influence of cationic substitutions on the oxygen loss and reversible capacity of lithium-rich layered oxide cathodes. Journal of Physical Chemistry C 2011; 115: 7097–7103.
16. Du J, Shan Z, Zhu K, *et al*. Improved electrochemical performance of $Li[Li_{0.2}Mn_{0.54}Ni_{0.13}Co_{0.13}]O_2$ by doping with molybdenum for lithium battery. Journal of Solid State Electrochemistry 2015; 19(4): 1037–1044.
17. Yu SH, Yoon T, Mun JY, *et al*. Continuous activation of $Li_2MnO_3$ component upon cycling in $Li_{1.167}Ni_{0.233}Co_{0.100}Mn_{0.467}Mo_{0.033}O_2$ cathode material for lithium-ion batteries. Journal of Materials Chemistry A 2013; 1: 2833–2839.
18. Li L, Song BH, Chang YL, *et al*. Retarded phase transition by fluorine doping in Li-rich layered $Li_{1.2}Mn_{0.54}Ni_{0.13}Co_{0.13}O_2$ cathode material. Journal of Power Sources 2015; 283: 162–170.
19. An J, Shi LY, Chen GR, *et al*. Insights into the stable layered structure of a Li-rich cathode material for lithium-ion batteries. Journal of Materials Chemistry A 2017; 5: 19728.
20. Li Z, Wang Z, Ban L, *et al*. Recent Advances on Surface Modification of Li- and Mn-Rich Cathode Materials. Acta Chim. Sinica 2019; 77: 1115.
21. Lim SN, Seo JY, Jung DS, *et al*. The crystal structure and electrochemical performance of $Li_{1.167}Mn_{0.548}Ni_{0.18}Co_{0.105}O_2$ composite cathodes doped and co-doped with Mg and F. Journal of Electroanalytical Chemistry 2015; 740: 88.
22. Hu S, Cheng G, Cheng M, *et al*. Cycle life im-

provement of $ZrO_2$-coated spherical $LiNi_{1/3}Co_{1/3}Mn_{1/3}O_2$ cathode material for lithium-ion batteries. Journal of Power Sources 2009; 188: 554.
23. Zheng JM, Li J, Zhang ZR, *et al*. The effects of $TiO_2$ coating on the electrochemical performance of $Li[Li_{0.2}Mn_{0.54}Ni_{0.13}Co_{0.13}]O_2$ cathode material for lithium-ion battery. Solid State Ionics 2008; 179(27–32): 1794–1799.
24. Zhang X, Belharouak I, Li L, *et al*. Structural and electrochemical study of $Al_2O_3$ and $TiO_2$ coated $Li_{1.2}Ni_{0.13}Mn_{0.54}Co_{0.13}O_2$ cathode material using ALD. Advanced Energy Materals 2013; 3: 1299–1307.
25. Wu Q, Yin Y, Sun S, *et al*. Novel $AlF_3$ surface modified spinel $LiMn_{1.5}Ni_{0.5}O_4$, for lithium-ion batteries: Performance characterization and mechanism exploration. Electrochimica Acta 2015; 158: 73–80.
26. Wu Y, Muruga VA, Manthiram A. Surface modification of high capacity layered $Li[Li_{0.2}Mn_{0.54}Ni_{0.13}Co_{0.13}]O_2$ cathodes by $AlPO_4$. Journal of the Electrochemical Society 2008; 155: A635.
27. Li CD, Yao ZL, Xu J, Tang P, Xiong X. Surface-modified $Li[Li_{0.2}Mn_{0.54}Ni_{0.13}Co_{0.13}]O_2$ nanoparticles with $LaF_3$ as cathode for Li-ion battery. Ionics 2017; 23: 549–558.
28. Ma D, Zhang P, Li Y, *et al*. $Li_{1.2}Mn_{0.54}Ni_{0.13}Co_{0.13}O_2$-encapsulated carbon nanofiber network cathodes with improved stability and rate capability for Li-ion batteries. Scientific Reports 2015; 5: 11257.
29. Xiang Y, Yin Z, Zhang Y, *et al*. Effects of synthesis conditions on the structural and electrochemical properties of the Li-rich material $Li[Li_{0.2}Ni_{0.17}Co_{0.16}Mn_{0.47}]O_2$ via the solid-state method. Electrochimica Acta 2013; 19: 214.
30. Chen Y, Xu G, Li J, *et al*. High capacity 0.5 $Li_2MnO_3 \cdot {}_{0.5}LiNi_{0.3}3Co_{0.33}Mn_{0.33}O_2$ cathode material via a fast co-precipitation method. Electrochimica Acta 2013; 87: 686.
31. Song C, Feng W, Su W, *et al*. Influence of the pH of li-rich $Li_{1.2}Mn_{0.54}Ni_{0.13}Co_{0.13}O_2$ on the electrochemical performance by sol–gel method. Integrated Ferroelectrics 2019; 200(1): 117–127.
32. Huang X, Zhang Q, Chang H, *et al*. Hydrothermal synthesis of nanosized $LiMnO_2$-$Li_2MnO_3$ compounds and their electrochemical performances. Journal of the Electrochemical Society 2009; 156(3): A162.
33. Li Z, Chernova NA, Feng J, *et al*. Stability and rate capability of Al substituted lithium-rich high-manganese content oxide materials for Li-ion batteries. Journal of the Electrochemical Society 2012; 159: A116.
34. Yan W, Xie Y, Jiang J, *et al*. Enhanced rate performance of Al-doped Li-rich layered cathode material via nucleation and post-solvothermal method. ACS Sustainable Chemistry & Engineering 2018; 6(4): 4625–4632.
35. Yahaya AH, Ibrahim ZA, Arof AK. Thermal, electrical and structural properties of $Li_2WO_4$. Journal of Alloys and Compounds 1996; 241(1–2): 148–152.
36. Nassau K, Glass AM, Grasso M, *et al*. Rapidly quenched tungstate and molybdate composition containing lithium: Glass formation and ionic conductivity. Journal of the Electrochemical Society 1980; 127(12): 2743.
37. Hayashi T, Okada J, Toda E, *et al*. Electrochemical effect of lithium tungsten oxide modification on $LiCoO_2$ thin film electrode. Journal of Power Sources 2015; 285: 559–567.
38. Hayashi T, Matsuda Y, Kuwata N, *et al*. High-power durability of $LiCoO_2$ thin film electrode modified with amorphous lithium tungsten oxide. Journal of Power Sources 2017; 354: 41–47.
39. Hayashi T, Miyazaki T, Matsuda Y, *et al*. Effect of lithium-ion diffusibility on interfacial resistance of $LiCoO_2$ thin film electrode modified with lithium tungsten oxides. Journal of Power Sources 2016; 305: 46–53.
40. Li X, Cao Z, Dong H, *et al*. Investigation of the structure and performance of $Li[Li_{0.13}Ni_{0.305}Mn_{0.565}]O_2$ Li-rich cathode materials derived from eco-friendly and simple coating techniques. RSC Advances 2020; 10(6): 3166–3174.
41. Yue P, Wang Z, Guo HJ, *et a*l. A low temperature fluorine substitution on the electrochemical performance of layered $LiNi_{0.8}Co_{0.1}Mn_{0.1}O_{2-z}F_z$ cathode materials. Electrochimical Acta 2013; 92: 1–8.
42. Nayak PK, Grinblat J, Levi M, *et al*. Al doping for mitigating the capacity fading and voltage decay of layered Li and Mn-rich cathodes for Li-ion batteries. Advanced Engineering Materials 2016; 6: 1502398–1502411.
43. Thackeray MM, Kang SH, Johnson CS, *et al*. $Li_2MnO_3$-stabilized $LiMO_2$ (M = Mn, Ni, Co) electrodes for lithium-ion batteries. Journal of Materials Chemistry 2007; 17(30): 3112–3125.
44. Zhen ZH, Li Q. Introduction to Rietveld refinement with X-ray power diffraction data GSAS software. Beijing: China Building Materials Press; 2016.
45. Guilmard M, Rougier A, Grüne M, *et al*. Effects of aluminum on the structural and electrochemical properties of $LiNiO_2$. Journal of Power Sources 2003; 115(2): 305–314.
46. Guo H, Xia Y, Zhao H, *et al*. Stabilization effects of Al doping for enhanced cycling performances of Li-rich layered oxides. Ceramics International 2017; 43(16): 13845–13852.